Faraday waves in smectic A liquid crystal layers

2010 J. Phys.: Condens. Matter 22 035106

(http://iopscience.iop.org/0953-8984/22/3/035106)

IOP Publishing Journal of Physics: Condensed Matter

J. Phys.: Condens. Matter **22** (2010) 035106 (8pp) doi:10.1088/0953-8984/22/3/035106

Faraday waves in smectic A liquid crystal layers

M Hernández-Contreras

Departamento de Física, Centro de Investigación y Estudios Avanzados del Instituto Politécnico Nacional, Apartado Postal 14-740, México Distrito Federal, Mexico

Received 8 September 2009, in final form 17 November 2009
Published 24 December 2009
Online at stacks.iop.org/JPhysCM/22/035106

Abstract

We studied with linear stability analysis the onset of parametric waves on the surface of a smectic A liquid crystal. For thin Sm-A layers under an applied static magnetic field there are subharmonic–harmonic branches of surface waves at low modulating frequency of the driving acceleration and long wavelength. A semi-infinite Sm-A medium poses a dispersion relation with similar trends as for Newtonian liquids. When the external forcing is negligible there are two damped surface waves excited by thermal fluctuation of the interface, whereas in the absence of a magnetic field the dominant modes are of harmonic type for typical material parameters.

1. Introduction

Faraday surface waves are generated on the surface of a liquid layer when it is subjected to vertical vibrational motion [1]. For a given frequency of the movement, once a critical driving acceleration is reached the surface develops an instability that leads to a series of stationary surface wave modes that form a rich variety of definite regular and crystalline geometric patterns [2–5]. The first theoretical analysis of these waves was performed by Benjamin and Ursell in the so-called linear stability regime [6]. They used an inviscid ideal fluid model and determined the forcing amplitude and wavenumber at onset as a function of the external frequency of excitation. The further extension of this theory to include Newtonian liquids [7] (for which the main waves are of subharmonic type occurring at half of the driving frequency) found excellent agreement for those properties with their corresponding study from the experimental counterpart [8]. Also, the same theoretical approach has been used to explain the Faraday surface wave as observed in viscoelastic fluids like semi-dilute polymeric [9–12], gels [13, 14] and wormlike micelle solutions [15] and ferrofluids [16, 17]. Yet, the validity of this linear theory to describe Faraday waves was recently demonstrated through comprehensive three-dimensional computer simulations on viscous fluids [18]. On the other hand, it has been determined experimentally that, due to interactions among the different wave modes, there appears a diversity of spatially symmetrical surface patterns which correspond to the nonlinear regime. These findings have motivated many experimental [2–5, 19] and theoretical studies [20–23] to characterize and understand these nonlinear waves in systems with lateral sizes comparable to the pattern's wavelength and also on model systems with infinite lateral extension. In particular, the weakly nonlinear theories advanced in [20, 21] for weakly viscous fluids have allowed explicit calculations of the effects of nonlinearities and of finite fluid depth [22] on pattern selection. However, to our knowledge similar studies for liquid crystals have not yet been undertaken. In contrast to the other complex fluids mentioned above, a comprehensive quantitative theoretical linear analysis of the dependence of the forcing acceleration and wavenumber on the strength of the external excitation frequency is still lacking for the Faraday instability in smectic A (Sm-A) liquid crystals. Therefore, in the present paper we report on our results of the adaptation of the linear theory approach to Faraday surface modes in limits appropriate to smectic A liquids under realistic fluid material properties.

We considered first a Sm-A layer under a constant horizontal magnetic field applied in the direction of the wavevector that orients the molecules in a stack of lamellar layers perpendicular to the air–liquid interface. In the most important region of linear analysis of low wavenumber and low frequency, we determined the dispersion relation and instability boundary (acceleration versus wavenumber curve) of surface waves in finite-thickness layers. We found that there are alternating subharmonic–harmonic unstable wave 'tongues' in the plot of the oscillation amplitude against wavenumber and for fixed frequency. In the important limiting case of this theory for unforced waves we provide the detailed form of the thermal surface mode power spectrum for semi-

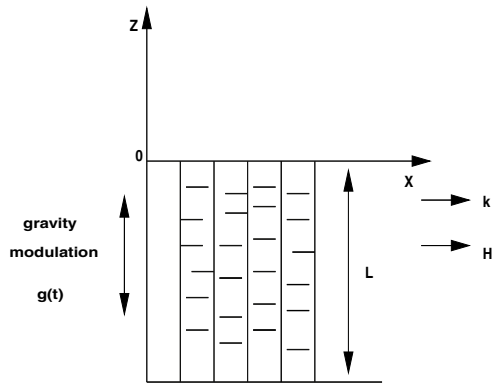

Figure 1. Smectic A liquid crystal under an applied static magnetic field H parallel to the wavevector $\mathbf{k}$ and to the Ox axis. The Sm-A lamellar layers are perpendicular to the free interface.

infinite unbounded Sm-A liquid crystals, and its dependence on the relevant fluid properties. Such spectral intensities of the surface displacement fluctuations are feasible to be measured with present-day surface light scattering techniques [24, 25]. In a second model system the liquid crystal layers are parallel to the vapor–fluid interface in the absence of a magnetic field. The predicted Faraday instability was found to exhibit enhanced wave responses with similar trends as in the first case above when the mode frequency is just a few Hertz and for very thin slabs of fluid.

2. First model: smectic A layers perpendicular to the surface in the presence of a horizontal magnetic field parallel to the wavevector

We consider a system made of vapor in contact with the fluid smectic layer of finite thickness L and infinite lateral extension. The material layer is subjected to a vertical sinusoidal vibration acceleration $g(t) = g - a\cos(wt)$, where a is the driving acceleration and w the frequency of oscillation, with g being the gravitational acceleration in a frame of reference co-moving with the container. ζ is the deformation shape of the interface due to normal displacements from its equilibrium configuration. An applied external horizontal magnetic field H orients the smectic A molecules in the x-axis direction while the stack of smectic layers remains perpendicular to the liquid–vapor interface, figure 1.

Due to symmetry in the xy plane of the spatial coordinates x and y we assume the generated surface wave propagates with wavevector $\mathbf{k}$ in the x direction, and therefore independently of the coordinate y. We characterize the elasticity of the interface by a surface tension γ. A splay module K determines the curvature distortion of surface deformation. B is a module of the layer's compression and χ_a is the magnetic susceptibility of the smectic molecules that are oriented by the applied magnetic field [26]. Thus, the elastic free energy of surface distortion is defined as [26, 27]

$$F = \tfrac{1}{2}\int \mathrm{d}^3\mathbf{r}\,\{B(\partial_x u)^2 + K(\partial_y^2 u + \partial_z^2 u)^2 + \chi_a H^2[(\partial_y u)^2 + (\partial_z u)^2]\}. \quad (1)$$

Here u is the displacement along the x axis perpendicular to the smectic layers and $\partial_\beta := \partial/\partial_\beta$, $\beta = x, y, z$.

The equation of motion giving the velocity about the basic state of rest, and in the moving frame, is

$$\rho\frac{\partial \mathbf{v}}{\partial t} = \nabla\cdot\boldsymbol{\sigma} + h\hat{\mathbf{e}}_z, \quad (2)$$

where $\boldsymbol{\sigma} = -p\mathbf{I} + \boldsymbol{\sigma}' + \boldsymbol{\sigma}^r - \rho g(t)\hat{\mathbf{e}}_z\hat{\mathbf{e}}_z$, with $(\mathbf{I})_{\alpha\beta} = 1$ if $\alpha = \beta$ and 0 otherwise. The molecular field

$$h = B\partial_x^2 u - K(\partial_z^4 u + 2\partial_{yz}^4 u + \partial_y^4 u) + \chi_a H^2(\partial_y^2 u + \partial_z^2 u). \quad (3)$$

The stress tensor

$$\boldsymbol{\sigma}' = \eta_2[\nabla\mathbf{v} + (\nabla\mathbf{v})^{\mathrm{T}}] + (\eta_3 - \eta_2)[\nabla(v_x\hat{\mathbf{e}}_x) + \partial_x\mathbf{v}\hat{\mathbf{e}}_x + (\nabla(v_x\hat{\mathbf{e}}_x) + \partial_x\mathbf{v}\hat{\mathbf{e}}_x)^{\mathrm{T}}] + \eta'\partial_x v_x\hat{\mathbf{e}}_x\hat{\mathbf{e}}_x, \quad (4)$$

where the viscosity $\eta' = \eta_1 + \eta_2 - 4\eta_3 - 2\eta_5 + \eta_4$ [27, 28], with $\hat{\mathbf{e}}_\alpha$ being a unit vector along the $\alpha = z, x$ axis, respectively. The deformation field u satisfies the bulk equation $\dot{u} - v_x = \lambda_p h$, where λ_p is the permeation length. p is the hydrostatic fluid pressure and ρ is the density.

For frequencies much less than the first sound frequencies of the solvent, the mass conservation equation in the incompressible limit is

$$\nabla\cdot\mathbf{v} = 0. \quad (5)$$

The equation of motion (2) is subjected to the boundary conditions at the material–vapor interface $z = 0$ where both the normal and shear stress must be independently in balance:

$$\sigma_{zz} = 0, \quad (6)$$

$$\sigma_{xz} = 0, \quad (7)$$

$$\sigma_{yz} = 0. \quad (8)$$

Using the free energy (1), the normal and tangential restoring forces are given by

$$\sigma_{zz}^{\mathrm{r}} = f_z = K\partial_x(\partial_y^2 + \partial_z^2)u + \gamma(\partial_x^2 + \partial_y^2)\zeta(x), \quad (9)$$

where we included in the last term the Laplace force due to the surface tension:

$$\sigma_{xz}^{\mathrm{r}} = f_x = K\partial_z(\partial_y^2 + \partial_z^2)u - \chi_a H^2\partial_z u. \quad (10)$$

$$\sigma_{yz}^{\mathrm{r}} = 0. \quad (11)$$

Linear stability of the flat interface requires that the surface elevation ζ be related to the velocity field v_z through the kinematic surface condition:

$$\partial_t\zeta = v_z, \qquad \text{at } z = 0, \quad (12)$$

and additionally is valid in the approximate relationship:

$$\frac{\partial u}{\partial z} = \frac{\partial\zeta}{\partial x}, \quad (13)$$

while it also satisfies the surface permeation equation:

$$\dot{u} - v_x = \frac{1}{\eta_3\kappa_s}f_x \quad (14)$$

with $\kappa_s^{-1} \approx 100$ Å a molecular length for the surface permeation [26]. For smectic A the surface equilibrium force at $z = 0$ [29] is

$$K\,\partial_x(\partial_x^2 u + \partial_z^2 u) = 0. \tag{15}$$

At the bottom of the container ($z = -L$) the no-slip boundary conditions

$$\mathbf{v} = \mathbf{0}, \tag{16}$$

and

$$\partial_z v_z = 0, \tag{17}$$

apply. Taking the double curl of equation (2) yields

$$\begin{aligned}-[\partial_t - \nu_2\nabla^2]\nabla^2 v_z &= (\nu_3 - \nu_2)\nabla^2[\partial_x\partial_z v_x - \partial_x^2 v_z] \\ &+ \nu'\partial_x^2\partial_x\partial_z v_x + \partial_x\partial_z\frac{h}{\rho}.\end{aligned} \tag{18}$$

Now, the divergence $\nabla_\perp := (\partial_x, \partial_y)$ of equation (2) and $\boldsymbol{\sigma}'$ lead to

$$\begin{aligned}\nabla_\perp^2 p &= [\rho\partial_t - \eta_2\nabla^2 - (\eta_3 - \eta_2)\partial_x^2]\partial_z v_z \\ &+ (\eta_3 - \eta_2)[\nabla_\perp^2 + \nabla^2]\partial_x v_x + \eta'\partial_x^2\partial_x v_x + \partial_x h,\end{aligned} \tag{19}$$

whereas balance of normal forces at the interface given by equation (6) yields an equation for the pressure, which together with (19) yields

$$\begin{aligned}&[\partial_t - \nu_2\nabla^2 - (\nu_3 - \nu_2)\partial_x^2 - 2\nu_2\nabla_\perp^2]\partial_z v_z \\ &= -(\nu_3 - \nu_2)[\nabla_\perp^2 + \nabla^2]\partial_x v_x - \nu'\partial_x^2\partial_x v_x \\ &- \frac{K}{\rho}\partial_x\nabla_\perp'^2\nabla_\perp^2 u + g(t)\nabla_\perp^2\zeta - \frac{\gamma}{\rho}\nabla_\perp^4\zeta - \frac{\partial_x h}{\rho},\end{aligned} \tag{20}$$

with $\nu_j = \eta_j/\rho$, $j = 2, 3$.

On the other hand, conditions (7) and (8) can be expressed as a single relationship:

$$\eta_3[\nabla_\perp^2 - \partial_z^2]v_z = [K\nabla_\perp'^2 - \chi_a H^2]\partial_x\partial_z u, \tag{21}$$

with $\nabla_\perp'^2 := \partial_y^2 + \partial_z^2$.

Thus, the Fourier transform of equations (18), (20), (21) and (3) provide respectively new forms for the above boundary conditions at $z = 0$:

$$\begin{aligned}&[\partial_t - \nu_2(\partial_z^2 - k^2)](\partial_z^2 - k^2)\tilde{v}_z \\ &= (\nu_3 - \nu_2)(-\partial_z^2 + k^2)[\mathrm{i}k\partial_z\tilde{v}_x + k^2\tilde{v}_z] \\ &+ \nu'\mathrm{i}k\partial_z\tilde{v}_x - \mathrm{i}k\partial_z\frac{\tilde{h}}{\rho},\end{aligned} \tag{22}$$

$$\begin{aligned}&[\partial_t + (\nu_3 + 2\nu_2)k^2 - \nu_2\partial_z^2]\partial_z\tilde{v}_z \\ &= -(\nu_3 - \nu_2)[-2\mathrm{i}k^3 + \mathrm{i}k\partial_z^2]\tilde{v}_x + \nu'\mathrm{i}k^3\tilde{v}_x \\ &+ \frac{\mathrm{i}K}{\rho}k^3\partial_z^2\tilde{u} - g(t)k^2\tilde{\zeta} - \frac{\gamma}{\rho}k^4\tilde{\zeta} - \frac{\mathrm{i}k\tilde{h}}{\rho},\end{aligned} \tag{23}$$

$$\eta_3[-k^2 - \partial_z^2]\tilde{v}_z = [K\partial_z^2 - \chi_a H^2]\mathrm{i}k\partial_z\tilde{u} = 0, \tag{24}$$

$$\tilde{h} = -Bk^2\tilde{u} - K\partial_z^4\tilde{u} + \chi_a H^2\partial_z^2\tilde{u}, \tag{25}$$

with $\mathrm{i} = \sqrt{-1}$ and $\tilde{u} = \int \mathrm{d}^2 r\, \mathrm{e}^{-\mathrm{i}\mathbf{k}\cdot\mathbf{r}}u$. In what follows we shall consider similarly the Fourier transform of the remaining conditions (12)–(17).

2.1. Floquet theory analysis

Since $g(t)$ is a periodic function with period $2\pi/w$, the solutions to equations (5), (12), (22) and (23) can be expressed according to Floquet's theory as superpositions of time-periodic functions [7, 13]:

$$\tilde{\zeta}(t) = \sum_{n=-\infty}^{\infty}\tilde{\zeta}_n \mathrm{e}^{\mu_n t}, \tag{26}$$

with $\mu_n(w) = \epsilon + \mathrm{i}(n + \alpha)w$, where ϵ and α are real-valued [7]. The surface wave will respond harmonically (H) to the driving frequency when $\alpha = 0$ and subharmonically (S) when $\alpha = 1/2$. Such an expansion is also performed on $\tilde{v}_z$ and $\tilde{v}_x$. Due to the reality condition on the above-mentioned displacement field, it turns out that $\tilde{\zeta}_n = \tilde{\zeta}_n^*$ with $\alpha = 0$, and $\tilde{\zeta}_n = \tilde{\zeta}_{n-1}^*$ for $\alpha = 1/2$. We now proceed to determine the coefficients $\tilde{\zeta}_n$.

Using the deformation field

$$\tilde{u}(z, t) = \sum_{n=-\infty}^{\infty}\tilde{u}_n(z)\mathrm{e}^{\mu_n t}, \tag{27}$$

and $\dot{u} - \tilde{v}_x = \lambda_p\tilde{h}$ in equation (22) we get a differential equation for the components of $\tilde{u}_n(z)$:

$$[\partial_z^8 - a_n\partial_z^6 + b_n\partial_z^4 - c_n\partial_z^2 + k^2 d_n]\tilde{u}_n(z) = 0, \tag{28}$$

where ∂_z^k, is the kth derivative with respect to z. The complex coefficients

$$\begin{aligned}a_n &= \frac{\mu_n}{\nu_3} + k^2\left(2 + \frac{\nu'}{\nu_3}\right) + \frac{1}{\xi_H^2} + \kappa^2, \\ b_n &= \frac{\mu_n}{\nu_3\xi_H^2} + k^2\left(\frac{\mu_n}{\nu_3} + \frac{2}{\xi_H^2} + \frac{1}{\lambda^2} + \frac{\nu'}{\nu_3\xi_H^2}\right) \\ &+ k^4 + \frac{\mu_n}{\lambda_p K} + \frac{\kappa^2}{\xi_H^2}, \\ c_n &= \frac{\mu_n^2}{\lambda_p K\nu_3} + k^2\left(\frac{\mu_n}{\lambda^2\nu_3} + \frac{\mu_n}{\xi_H^2\nu_3} + \frac{2\mu_n}{\lambda_p K}\right. \\ &\left. + \frac{\nu'\mu_n}{\nu_3\lambda_p K} + \frac{\kappa^2}{\lambda^2}\right) + k^4\left(\frac{1}{\xi_H^2} + \frac{2}{\lambda^2} + \frac{\nu'}{\nu_3\lambda^2}\right), \\ d_n &= \frac{\mu_n^2}{\lambda_p K\nu_3} + k^2\left(\frac{\mu_n}{\lambda^2\nu_3} + \frac{\mu_n}{\lambda_p K}\right) + \frac{k^4}{\lambda^2},\end{aligned} \tag{29}$$

where $\xi_H = \sqrt{K/\chi_a}/H$, $\lambda = \sqrt{K/B}$, $\lambda_p = 1/(\rho\nu_3\kappa^2)$ and $\nu' = \eta'/\rho$. Solutions to equation (28) are of the general form $\tilde{u}_n(z) \sim \mathrm{e}^{\theta(k)z}$. Thus, an algebraic equation is obtained when the change of variable $S = \theta^2$ is made:

$$S^4 - a_n S^3 + b_n S^2 - c_n S + k^2 d_n = 0, \tag{30}$$

where all modes S_j, $j = 1, \ldots, 4$ can be calculated numerically from equation (30). However, the approximated analytical solution mode $S_1 \approx k^2 d_n/c_n$ was found to be valid

at long-wavelength $\lambda k \ll 1$ and low-frequency $w < B/\eta_3$, $w < k\sqrt{B/\rho}$ limits [30, 31].

The most general solution can be written as

$$\tilde{u}_n(z) = \sum_{j=1}^{4} [A_j e^{z\sqrt{S_j}} + B_j e^{-z\sqrt{S_j}}]. \tag{31}$$

It is now possible to define both $\tilde{v}_z$ and $\tilde{v}_x$ in terms of A_j, B_j with help of the expressions $\dot{u} - \tilde{v}_x = \lambda_p \tilde{h}$ and (5). Equation (12) gives the displacement field $\tilde{\zeta}$ as a function of the constants A_j, B_j, $j = 1, \ldots, 4$, which in turn can be determined from the kinematic relationship and boundary conditions, equations (12)–(17) and equations (22)–(25). A numerical estimation of their magnitudes leads to the inequality $|A_1|, |B_1| \gg |A_j|, |B_j|$, $j = 2, 3, 4$ in a wide range of parameter values defining different model smectic A systems [26, 30]. For instance, when $k \sim 10^4$ m^{-1}, $K \sim 10^{-11}$–10^{-7} N, $B \sim 10^6$–10^3 N m^{-2}, $w \sim 1$–10^2 Hz, layer thickness $L = 10^{-2}$–10^{-3} m, $\lambda_p = 10^{-14}$–10^{-17} m^4 N^{-1} s^{-1}, $\rho = 10^3$ kg m^{-3}, $\eta_3 = 1$ P, $\eta' = \eta_2 = \eta_3$, $\chi_a = 10^{-8}$ kg m^{-1} s^{-2} G^{-2}, $H = 3000$ G, $\gamma = 0.033$ N m^{-1}.

It should be noted that the explicit values of the constants A_1, B_1 can be written as a function of the modes $\tilde{\zeta}_n$.

Thus, we determined these two constants from the above boundary conditions. By means of equations (5), (12), (13) and (16) which together constitute a single boundary condition on A_1 and B_1, and with the help of equation (26), we found their values as a function of $\tilde{\zeta}_n$ only (see equations (70) and (71) in the appendix). Therefore, using this solution in equation (23) we get the recursion relationship for all the interface displacement components $\tilde{\zeta}_n$:

$$M_n \tilde{\zeta}_n = a(\tilde{\zeta}_{n-1} + \tilde{\zeta}_{n+1}), \tag{32}$$

$$\begin{aligned} M_n = \frac{2}{k}\Bigg\{ w_0^2 + \Bigg\{ & \frac{[Bk^2 + KS_1^2 + Kk^2 S_1 + \chi_a H^2 S_1]}{\rho} \\ & + [\mu_n + \lambda_p B k^2 + \lambda_p (KS_1^2 - \chi_a H^2 S_1)] \\ & \times [\mu_n + k^2(3\nu_3 + \nu') - \nu_3 S_1] \Bigg\} \frac{(A_1 + B_1)}{i\tilde{\zeta}_n} \Bigg\} \\ \equiv \frac{2}{k} D_n^L(k, \mu_n = iw), \end{aligned} \tag{33}$$

with

$$w_0^2 = gk + \frac{\gamma k^3}{\rho}. \tag{34}$$

$$\begin{aligned} A_1 = {} & \frac{\tilde{\zeta}_n i e^{L\sqrt{S_1}}}{2k\sqrt{S_1} R_n} (-1 + \coth(L\sqrt{S_1})) \\ & \times \{\mu_n S_1 + k^2(-1 + e^{L\sqrt{S_1}}) R_n\}, \\ B_1 = {} & \frac{\tilde{\zeta}_n i}{(-1 + e^{L\sqrt{S_1}}) k\sqrt{S_1} R_n} \\ & \times \{\mu_n S_1 e^{L\sqrt{S_1}} - k^2(-1 + e^{L\sqrt{S_1}}) R_n\}, \\ R_n = {} & \lambda_p B K^2 + \lambda_p K S_1^2 - \lambda_p \chi_a H^2 S_1 + \mu_n. \end{aligned} \tag{35}$$

$$\begin{aligned} M_n^\infty = {} & \frac{2}{k}\Bigg\{ w_0^2 + \frac{k}{\sqrt{S_1}} \frac{[Bk^2 + KS_1^2 + Kk^2 S_1 + \chi_a H^2 S_1]}{\rho} \\ & + \frac{k}{\sqrt{S_1}} \mu_n [\mu_n + k^2(3\nu_3 + \nu') - \nu_3 S_1] \Bigg\} \\ \equiv {} & \frac{2}{k} D_n^\infty(k, \mu_n = iw), \end{aligned} \tag{36}$$

where we used $\lambda_p \approx 0$.

2.2. Linear stability analysis

In the presence of the external acceleration $a \neq 0$ there is coupling among different temporal modes. Therefore we resort to a numerical solution of equation (32) for a finite value $n = N$ to yield the stability analysis of the free surface. Thus, equation (32) reduces to an eigenvalue problem with eigenvalue a and complex eigenvectors determined by $\vec{\zeta}$ [7, 13]. For that purpose it is convenient to rewrite equation (32) for the harmonic and subharmonic cases separately as

$$\mathbf{M}\vec{\zeta} = a\mathbf{U}_H\vec{\zeta}, \qquad \text{and} \qquad \mathbf{M}\vec{\zeta} = a\mathbf{U}_S\vec{\zeta}, \tag{37}$$

where $\mathbf{M}$, $\mathbf{U}_H$ and $\mathbf{U}_S$ are real matrices of order $2(N+1) \times 2(N+1)$ and $\vec{\zeta}$ is a vector of order $2(N+1)$:

$$\vec{\zeta} = \begin{pmatrix} \tilde{\zeta}_0^r \\ \tilde{\zeta}_0^i \\ \tilde{\zeta}_1^r \\ \tilde{\zeta}_1^i \\ \tilde{\zeta}_2^r \\ \tilde{\zeta}_2^i \\ \vdots \end{pmatrix}. \tag{38}$$

Here the complex numbers $M_n = M_n^r + iM_n^i$, $\tilde{\zeta}_n = \tilde{\zeta}_n^r + i\tilde{\zeta}_n^i$, $n = 0, 1, \ldots, N+1$:

$$\mathbf{M} = \begin{pmatrix} M_0^r & -M_0^i & 0 & 0 & 0 & 0 & \ldots \\ M_0^i & M_0^r & 0 & 0 & 0 & 0 & \ldots \\ 0 & 0 & M_1^r & -M_1^i & 0 & 0 & \ldots \\ 0 & 0 & M_1^i & M_1^r & 0 & 0 & \ldots \\ 0 & 0 & 0 & 0 & M_2^r & -M_2^i & \ldots \\ 0 & 0 & 0 & 0 & M_2^i & M_2^r & \ldots \\ \vdots & \vdots & \vdots & \vdots & \vdots & \vdots & \ddots \end{pmatrix}, \tag{39}$$

and

$$\mathbf{U}_H = \begin{pmatrix} 0 & 0 & 2 & 0 & 0 & 0 & \ldots \\ 0 & 0 & 0 & 0 & 0 & 0 & \ldots \\ 1 & 0 & 0 & 0 & 1 & 0 & \ldots \\ 0 & 1 & 0 & 0 & 0 & 1 & \ldots \\ 0 & 0 & 1 & 0 & 0 & 0 & \ldots \\ 0 & 0 & 0 & 1 & 0 & 0 & \ldots \\ \vdots & \vdots & \vdots & \vdots & \vdots & \vdots & \ddots \end{pmatrix}, \tag{40}$$

$$\mathbf{U}_S = \begin{pmatrix} 1 & 0 & 1 & 0 & 0 & 0 & \ldots \\ 0 & -1 & 0 & 1 & 0 & 0 & \ldots \\ 1 & 0 & 0 & 0 & 1 & 0 & \ldots \\ 0 & 1 & 0 & 0 & 0 & 1 & \ldots \\ 0 & 0 & 1 & 0 & 0 & 0 & \ldots \\ 0 & 0 & 0 & 1 & 0 & 0 & \ldots \\ \vdots & \vdots & \vdots & \vdots & \vdots & \vdots & \ddots \end{pmatrix}. \tag{41}$$

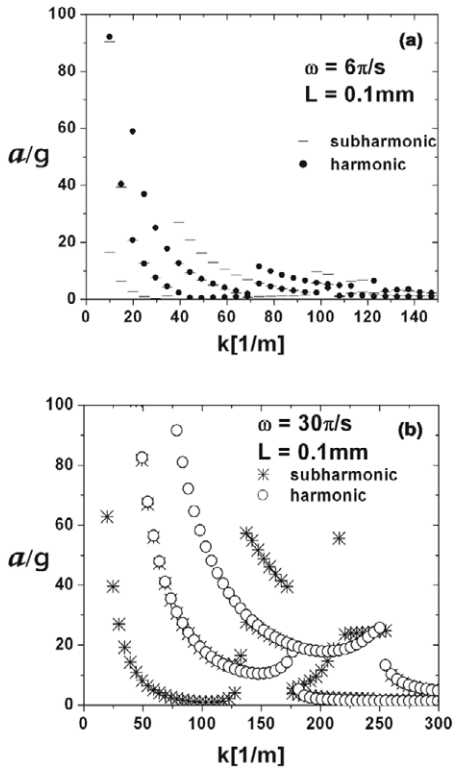

Figure 2. Neutral stability curves of Faraday waves for the smectic A liquid crystal under an applied static magnetic field $H = 3000$ G parallel to the wavevector **k** and to the equilibrium vapor–liquid interface. Magnetic susceptibility of the molecules $\chi_a = 10^{-8}$ kg m^{-1} s^{-2} G^{-2}. Figure 2(a) for modulation frequency $w = 6\pi$ s^{-1}, whereas 2(b) with $w = 30\pi$ s^{-1}. Other system's parameters are given in section 2.2 and were kept constant and equal in the two cases considered. The Sm-A lamellar layers are perpendicular to the free interface.

Solution of this eigenvalue problem for $\epsilon = 0$ yields the neutral stability curve $a(k, w)$ for a given wavenumber k corresponding to fixed material parameters of the liquid crystal. We follow the approach given by Kumar [7] and Kumar [13].

In figure 2 are given the calculated wave zones against wavenumber for two frequencies: figure 2(a) with $w = 6\pi$ s^{-1} and figure 2(b) for $w = 30\pi$ s^{-1}. The material parameters defining the model system are; $K = 10^{-11}$ N, $B = 10^6$ N m^{-2}, layer thickness $L = 10^{-4}$ m, $\lambda_p = 10^{-14}$ m^4 N^{-1} s^{-1}, $\rho = 10^3$ kg m^{-3}, $\eta_3 = 1$ P, $\eta_2 = \eta_3$, $\eta' = 10^{-2}\eta_3$, $\chi_a = 10^{-8}$ kg m^{-1} s^{-2} G^{-2}, $H = 3000$ G and $\gamma = 0.033$ N m^{-1}.

Figure 2(a) depicts first the subharmonic waves from low wavenumbers up to $k \sim 40$ m^{-1} (dashed line), which is then followed by the region of harmonic waves (black filled circles). These very well-defined alternating regions of Faraday waves are obtained mainly at a low ratio of driving to gravitational accelerations a/g, and from low up to $k = 100$ m^{-1}. At this low frequency, $w = 6\pi$ s^{-1}, the minimum amplitude acceleration is $a = 0$. That is, modes of different branches can be excited for infinitesimal values of a in much the same way as happens on an ideal inviscid fluid [6, 7]. Figure 2(b) corresponds to the same system of figure 2(a) where, however, we have only increased the frequency. It is noted that the alternating pattern of subharmonic–harmonic waves of

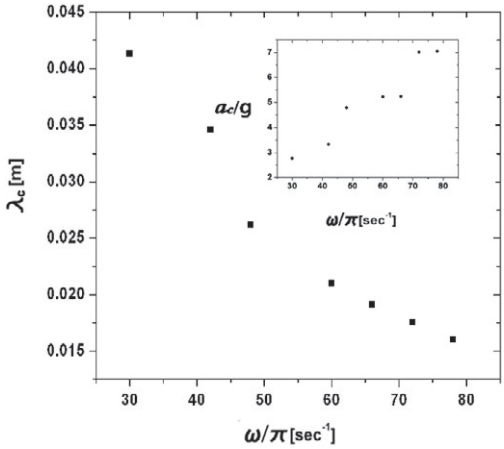

Figure 3. Calculated dispersion relation for a semi-infinite Sm-A liquid crystal in the long wavelength and low frequency limits. Same fluid parameters as in figure 2. The inset shows the critical amplitude of oscillation versus frequency.

figure 2(a) shifts to higher values of k and is characterized by a meaningful wider range of nonzero a/g values. From the numerical solution of equation (32) for the vapor–liquid semi-infinite medium, equation (36), we obtained the critical wavelength λ_c and amplitude of oscillation a_c as a function of frequency, which are depicted in figure 3. They are of the same order of magnitude as compared to a glycerin–water mixture in air [32]. This could be useful to estimate the elastic constants and viscosity of an Sm-A liquid from their fit to experimental data.

2.3. Thermal waves

We note that, for $a = 0$ and $n = 0$, $D_n^L(k, \mu_n = \mathrm{i}w) = 0$ is the dispersion relation of a finite-thickness layer experiencing thermal surface waves, whereas its semi-infinite medium version $L \to \infty$ is given by $D_{n=0}^{\infty}(k, \mu_n = \mathrm{i}w) = 0$. Such relationships have not been reported before in the literature. Surface light scattering measures the power spectrum $S(k, w)$ of the fluctuating interface of a semi-infinite medium. It can be recast into an equation for the local surface displacement $\tilde{\zeta}$ by means of the fluctuation–dissipation theorem [25]:

$$S(k, w) = \langle|\tilde{\zeta}(k, w)|^2\rangle = \frac{k_B T}{\pi w}\,\mathrm{Im}[\chi(k, w)], \qquad (42)$$

where

$$\zeta(\mathbf{r}, t) = \int_{\mathrm{Area}} \mathrm{d}^2\mathbf{r}' \int P^{\mathrm{ext}}(\mathbf{r} - \mathbf{r}', t - \tau)\chi(\mathbf{r}', \tau)\,\mathrm{d}\tau, \qquad (43)$$

and P^{ext} is a weakly applied external pressure on the interface. For $L \to \infty$ the dissipative function $\chi = 2/\rho D_{n=0}^{\infty}$. We found two viscous damped modes, see figure 4.

In the region of small frequency $\lambda_p B k^2 \ll w \ll \nu_3 k^2 \ll k\sqrt{B/\rho}$ and $\lambda k \ll 1$ the mode $\sqrt{S_1} \approx \kappa^{-1}k^2\sqrt{\frac{w}{2\lambda_p Bk^2}}[1 + \lambda_p Bk^2/2w + \mathrm{i}(1 - \lambda_p Bk^2/2w)]$, it yields from equation (42)

$$S(k, w) = \frac{k_B T}{2w\pi}\,\frac{\kappa^{-1}k^2\sqrt{\frac{2w}{\lambda_p Bk^2}}}{Den1} \qquad (44)$$

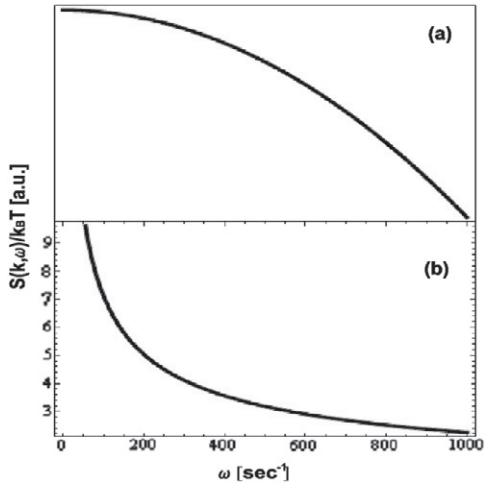

Figure 4. Power spectrum of damped thermal waves on the free surface of a semi-infinite medium of Sm-A liquid crystal. Same parameters as in figure 2. (a) Plot of equation (44) and (b) from equation (46).

$$Den1 = Bk^2 + \gamma\kappa^{-1}k^4\left(1 + \frac{\lambda_p Bk^2}{2w}\right)\sqrt{\frac{2w}{\lambda_p Bk^2}}. \quad (45)$$

Finally, we determined another region where thermal waves can be found: $w \ll \lambda_p Bk^2 \ll \nu_3 k^2 \ll k\sqrt{B/\rho}$, where the mode $\sqrt{S_1} \approx \kappa^{-1}k^2(1 + \mathrm{i}w/2\lambda_p Bk^2)$, with $\mu_n = \mathrm{i}w$ and

$$S(k, w) = \frac{k_B T}{2\pi\lambda_p Bk^2}\frac{[Bk^2 - \kappa^{-1}k(Kk^4 - \chi_a H^2 k^2)]}{Den2}, \quad (46)$$

$$\begin{aligned} Den2 &= (\gamma k^3 + Bk^2(\kappa^{-1}k)^{-1})^2 + \left(\frac{\gamma k^3 w}{2\lambda_p Bk^2}\right)^2 \\ &\times \left[2(\gamma k^3 + Bk^2(\kappa^{-1}k)^{-1}) + \frac{\gamma k^3 w^2}{(\lambda_p Bk^2)^2}\right] \\ &\times \kappa^{-1}k(Kk^4 - \chi_a H^2 k^2) \\ &+ \left(1 + \frac{w^2}{(\lambda_p Bk^2)^2}\right)(\kappa^{-1}k)^2(Kk^4 - \chi_a H^2 k^2)^2. \end{aligned} \quad (47)$$

3. Second model: smectic A layers parallel to the surface with no magnetic field

Our second model system consists of a smectic A liquid crystal of thickness L that is formed by a lamellar stack of equally spaced parallel layers with deformation field u perpendicular to the liquid–vapor interface and oriented along the z axis, figure 5.

The bulk elastic free energy of smectic A is [14, 27]

$$F = \tfrac{1}{2}\int \mathrm{d}^3\mathbf{r}\,\{B(\partial_z u)^2 + K(\partial_x^2 u + \partial_y^2 u)^2\}. \quad (48)$$

Note that in this case the stress tensor is defined by

$$\begin{aligned} \boldsymbol{\sigma}' &= \eta_2[\nabla\mathbf{v} + (\nabla\mathbf{v})^{\mathrm{T}}] + (\eta_3 - \eta_2)[\nabla(v_z\hat{\mathbf{e}}_z) + \partial_z\mathbf{v}\hat{\mathbf{e}}_z \\ &+ (\nabla(v_z\hat{\mathbf{e}}_z) + \partial_z\mathbf{v}\hat{\mathbf{e}}_z)^{\mathrm{T}}] + \eta'\partial_z v_z\hat{\mathbf{e}}_z\hat{\mathbf{e}}_z, \end{aligned} \quad (49)$$

whereas the displacement u satisfies

$$\partial_t u = v_z + \lambda_p h, \quad (50)$$

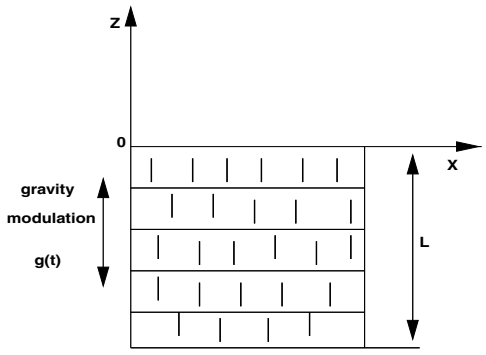

Figure 5. Smectic A configuration and coordinate system used.

with

$$h = B\partial_z^2 u - K\nabla_\perp^2\nabla_\perp^2 u. \quad (51)$$

The general elastic forces on the interface become now [27, 30, 31]

$$\sigma_{zz}^{\mathrm{r}} = f_z = B\partial_z u + \gamma(\partial_x^2 + \partial_y^2)\zeta(x), \quad (52)$$

where the second term takes into account the capillary force component

$$\sigma_{xz}^{\mathrm{r}} = f_x = -K\partial_x\nabla_\perp^2 u, \quad (53)$$

$$\sigma_{yz}^{\mathrm{r}} = f_y = -K\partial_y\nabla_\perp^2 u, \quad (54)$$

where $\nabla_\perp^2 := \partial_x^2 + \partial_y^2$.

Using similar methods of section 2 we obtain the dynamical equations for the velocity component v_z:

$$[\partial_t - \nu_3\nabla^2]\nabla^2 v_z = \nu'\nabla_\perp\partial_z^2 v_z + \nabla_\perp^2\frac{h}{\rho}, \quad (55)$$

$$\begin{aligned} &[\partial_t - (3\nu_3 + \nu')\nabla_\perp^2 - \nu_3\partial_z^2]\partial_z v_z \\ &= \frac{B}{\rho}\nabla_\perp^2\partial_z u + g(t)\nabla_\perp^2\zeta - \frac{\gamma}{\rho}\nabla_\perp^2\nabla_\perp^2\zeta, \end{aligned} \quad (56)$$

$$\eta_3[\nabla_\perp^2 - \partial_z^2]v_z = K\nabla_\perp^2\nabla_\perp^2 u, \quad (57)$$

and their Fourier transforms at $z = 0$ are

$$(\partial_t - \nu_3[\partial_z^2 - k^2])(\partial_z^2 - k^2)\tilde{v}_z = -\nu' k^2\partial_z^2\tilde{v}_z - k^2\frac{\tilde{h}}{\rho}, \quad (58)$$

$$\begin{aligned} &[\partial_t + (3\nu_3 + \nu')k^2 - \nu_3\partial_z^2]\partial_z\tilde{v}_z \\ &= -\frac{B}{\rho}k^2\partial_z\tilde{u} - \left[g(t) + \frac{\gamma}{\rho}k^2\right]k^2\tilde{\zeta}, \end{aligned} \quad (59)$$

$$\eta_3[k^2 + \partial_z^2]\tilde{v}_z = -Kk^4\tilde{u}, \quad (60)$$

$$h = B\partial_z^2\tilde{u} - Kk^4\tilde{u}. \quad (61)$$

The displacement field $\tilde{u}_n$ fulfills the differential equation

$$[\partial_z^6 - a_n'\partial_z^4 + b_n'\partial_z^2 - c_n']\tilde{u}_n(z) = 0, \quad (62)$$

where

$$a'_n = k^2\left[\frac{\mu_n}{\lambda_p Bk^2}\left(1+\frac{\lambda_p B}{\nu_3}\right)+\lambda^2k^2+2+\frac{\nu'}{\nu_3}\right],$$
$$b'_n = k^4\left[\left(\frac{\mu_n}{\lambda_p Bk^2}+\lambda^2k^2\right)\left(\frac{\mu_n}{\nu_3k^2}+2+\frac{\nu'}{\nu_3}\right)+\frac{\mu_n}{\nu_3k^2}+\frac{1}{\rho\nu_3\lambda_pk^2}+1\right], \quad (63)$$
$$c'_n = k^6\left[\left(\frac{\mu_n}{\lambda_p Bk^2}+\lambda^2k^2\right)\left(\frac{\mu_n}{\nu_3k^2}+1\right)+\frac{\lambda^2}{\rho\nu_3\lambda_p}\right].$$

Now the assumption $\tilde{u}_n(z) \sim e^{\theta(k)z}$ and $S = \theta^2$ lead to

$$S^3 - a'_nS^2 + b'_nS - c'_n = 0. \quad (64)$$

Since $\tilde{u}_n$ has the general form of expression (31), and on using (50) it results in Floquet's form of $\tilde{v}_z = \sum_n \tilde{w}_n(z)e^{\mu_n t}$:

$$\tilde{w}_n(z) = \sum_{j=1}^{3}(\mu_n - \lambda_p[BS_j - Kk^4]) \times [A_je^{z\sqrt{S_j}} + B_je^{-z\sqrt{S_j}}]. \quad (65)$$

The solution modes S_j of (64) can be determined fully numerically. We found nevertheless that they can be approximated at low frequency and long wavelength [30, 34]. In this case

$$S_1 = k^2\frac{\frac{B}{\eta_3}(\lambda k)^2+\mu_n+\frac{\mu_n^2}{\nu_3k^2}}{\frac{B}{\eta_3}+\mu_n(2+\frac{\nu'}{\nu_3})+\frac{\mu_n^2}{\nu_3k^2}}, \quad (66)$$

$$S_{2,3} = \tfrac{1}{2}\left[a'_n \mp \sqrt{(a'_n)^2-4b'_n}\right]. \quad (67)$$

However, the boundary conditions imply that $|A_1|, |B_1| \gg |A_j|, |B_j|$, $j = 2, 3$ and the smallness of $\lambda_p \approx 0$ allows us to derive a simple expression for the components $\tilde{\zeta}_n$ of a finite-thickness Sm-A layer in terms of only one mode, S_1. Thus

$$M_n\tilde{\zeta}_n = a(\tilde{\zeta}_{n-1}+\tilde{\zeta}_{n+1}), \quad (68)$$

where now M_n is defined as

$$M_n = \frac{2}{k}\left\{w_0^2+\left(\frac{Bk\sqrt{S_1}}{\rho}+\frac{\sqrt{S_1}}{k}\mu_n[\mu_n+k^2(3\nu_3+\nu')-\nu_3S_1]\right)\coth(L\sqrt{S_1})\right\}, \quad (69)$$

$w_0^2 = gk+\gamma k^3/\rho$. Our expression of equation (69) with $n = 0$ coincides with the dispersion relation of thermal waves on Sm-A found by other authors [30, 33, 34].

Figure 6 is the plot of the ratio of the external driving to constant gravity acceleration a/g versus wavenumber k. The material parameters of this system are; $K = 10^{-10}$ N, $B = 10^4$ N m^{-2}. Layer thicknesses $L = 0.05$, 0.05, 0.03 m, frequencies $w = 6\pi$ s^{-1}, 18π s^{-1} and 18π s^{-1} corresponding to figures 6(a), (b) and (c), respectively. $\lambda_p = 10^{-14}$ m^4 N^{-1} s^{-1}, $\rho = 10^3$ kg m^{-3}, $\eta_3 = 1$ P, $\eta_2 = \eta_3$, $\eta' = 10^{-2}\eta_3$ and $\gamma = 0.033$ N m^{-1}.

From figure 6(a) we can observe that for increasing values of wavenumber the first instability is subharmonic

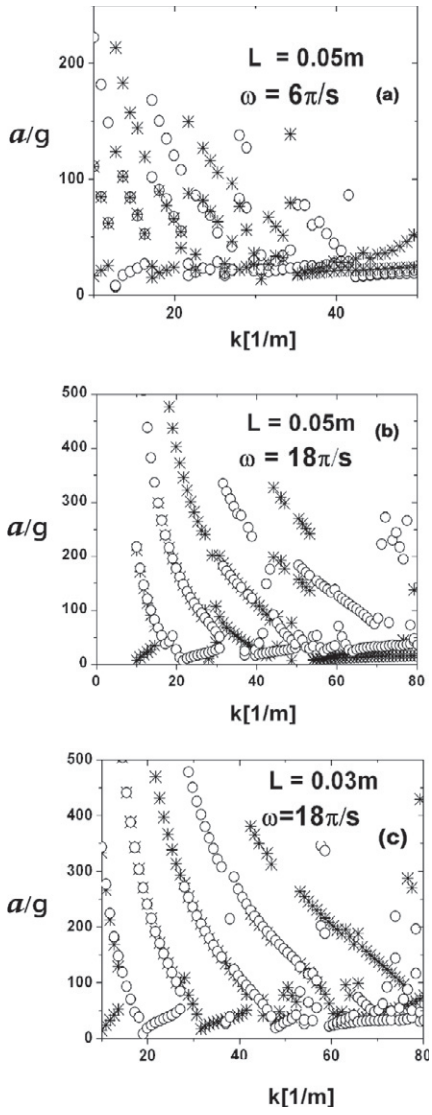

Figure 6. Neutral stability curves of Faraday waves given as the ratio a/g against wavenumber k. There is no applied magnetic field. The subharmonic branch is depicted with star symbol $*$ and harmonic branch with $\circ$. Fluid parameters are given in section 3. The Sm-A lamellar layers are parallel to the liquid–vapor interface.

(star symbols) then followed by a harmonic one (white circle symbols). This pattern of instabilities is well defined only in a small window of wavenumbers, $0 < k < 30$ m^{-1}. For low frequency $w = 6\pi$ s^{-1}, it is possible to find harmonic waves that are favored first, with a lower critical acceleration of $a_c/g \approx 7.31$ for $k \approx 12.7$ m^{-1}, than subharmonic ones which have $a_c/g \approx 16$ for any fixed k. (The critical amplitude a_c is the minimum of $a(k, w)$ for the lowest branch [32].) Further increase of the frequency up to $w = 18\pi$ s^{-1} as shown in figure 6(b) reduces the strength of a_c and a of both branches, making them converge roughly to the same magnitude $a/g \approx 7$ but with different wavenumbers. The layer thickness effect was determined from figure 6(b) corresponding to $L = 0.05$ m and its comparison with figure 6(c) where we used a smaller thickness $L = 0.03$ m and the same frequency $w = 18\pi$ s^{-1} while the other parameters remained fixed. In this case, the minimum critical acceleration corresponds to the harmonic

branch, whereas the subharmonic–harmonic neutral stability curve regions grow, becoming better defined compared to those from the larger thickness system of figure 6(b).

4. Conclusions

We found that Faraday waves develop in thin (0.1 mm, 0.05 m) smectic A liquid crystal layers at low frequencies of external driving acceleration and in the long wavelength limit. For Sm-A under an external magnetic field, and for typical material parameters, there are alternating subharmonic–harmonic branches with almost the same vanishing critical excitation acceleration as occurs in ideal inviscid fluids. An increase of the modulating frequency makes the subharmonic waves to preempt the harmonic ones with a lower onset nonzero acceleration. In the case of an Sm-A semi-infinite medium, the dispersion relation exhibits similar behavior to Newtonian liquids, showing the same order of magnitude for the amplitude of oscillation and wavenumber. For zero forcing acceleration we provide the power spectrum of damped surface waves excited by thermal fluctuations. However, in the case of Sm-A at zero magnetic field, harmonic waves can be the dominant instability having lower critical acceleration than subharmonic waves mainly for low frequencies and thicker layers of Sm-A than when the magnetic field is present.

Acknowledgments

This work was supported by CONACyT grant nos. 48794-F and 60595, México.

Appendix

From equations (12) and (16) we get

$$\{\mu_n S_1 - k^2[\mu_n + \lambda_p B k^2 + \lambda_p (K S_1^2 - \chi_a H^2 S_1)] \times (1 - e^{-L\sqrt{S_1}})\} A_1 + \{-\mu_n S_1 + k^2[\mu_n + \lambda_p B k^2 + \lambda_p (K S_1^2 - \chi_a H^2 S_1)](1 - e^{L\sqrt{S_1}})\} B_1 = 0, \quad (70)$$

and from equation (13) it results in

$$\{\mu_n + \lambda_p B k^2 + \lambda_p (K S_1^2 - \chi_a H^2 S_1)\} \times \frac{(1 - e^{-L\sqrt{S_1}})}{\sqrt{S_1}} A_1 - \{\mu_n + \lambda_p B k^2 + \lambda_p (K S_1^2 - \chi_a H^2 S_1)\} \frac{(1 - e^{L\sqrt{S_1}})}{\sqrt{S_1}} B_1 = \frac{i \mu_n \tilde{\zeta}_n}{k}. \quad (71)$$

References

[1] Faraday M 1831 *Phil. Trans. R. Soc. Lond.* **121** 299
[2] Christiansen B, Alstrom P and Levinson M T 1992 *Phys. Rev. Lett.* **68** 2157
[3] Edwards W S and Fauve S 1994 *J. Fluid Mech.* **278** 123
[4] Kudrolli A, Pier P and Gollub J P 1998 *Physica* D **123** 99
[5] Arbell H and Fineberg J 1998 *Phys. Rev. Lett.* **81** 4384
[6] Benjamin T and Ursell F 1954 *Proc. R. Soc.* A **225** 505
[7] Kumar K and Tuckerman L 1994 *J. Fluid Mech.* **279** 49
[8] Bechhoefer J, Ego V, Manneville S and Johnson B 1995 *J. Fluid Mech.* **288** 325
[9] Müller H W and Zimmermann W 1999 *Europhys. Lett.* **45** 169
[10] Wagner C, Müller H W and Knorr K 1999 *Phys. Rev. Lett.* **83** 308
[11] Kumar S 2002 *Phys. Rev.* E **65** 026305
[12] Raynal F, Kumar S and Fauve S 1999 *Eur. Phys. J.* B **9** 175
[13] Kumar S 1999 *Phys. Fluids* **11** 1970
[14] Ovando-Vázquez C, Vázquez Rodriguez O and Hernández-Contreras M 2008 *AIP Conf. Proc.* **1077** 135
[15] Ballesta P and Manneville S 2005 *Phys. Rev.* E **71** 026308
[16] Müller H W 1998 *Phys. Rev.* E **58** 6199
[17] Mekhonoshin V V and Lange A 2002 *Phys. Rev.* E **65** 061509
[18] Périnet N, Juric D and Tuckerman L S 2009 arXiv:0901.0464
[19] Kityk A V, Embs J, Mekhonoshin V V and Wagner C 2009 *Phys. Rev.* E **79** 029902(E)
[20] Zhang W and Viñals J 1997 *J. Fluid. Mech.* **336** 301
[21] Chen P and Viñals J 1999 *Phys. Rev.* E **60** 559
[22] Skeldon A C and Guidoboni G 2007 *SIAM J. Appl. Maths.* **67** 1064
[23] Silber M, Topaz C and Skeldon A C 2000 *Physica* D **143** 205
[24] Monroy F and Langevin D 1998 *Phys. Rev. Lett.* **81** 3167
[25] Langevin D 1992 *Scattering by Liquid Surfaces and Complementary Techniques* (New York: Dekker)
[26] Langevin D 1976 *J. Physique* **37** 737
[27] de Gennes P G and Prost J 1993 *The Physics of Liquid Crystals* (Oxford: Clarendon)
[28] Martin P C, Parodi O and Persham P S 1972 *Phys. Rev.* A **6** 2401
[29] Kléman M and Parodi O 1975 *J. Physique* **36** 617
[30] Chen H Y and Jasnow D 1998 *Phys. Rev.* E **57** 5639
[31] Fedorov D O, Romanov V P and Ul'yanov S V 2000 *Phys. Rev.* E **62** 681
[32] Kumar K 1996 *Proc. R. Soc.* A **452** 1113
[33] Chen H Y and Jasnow D 2000 *Phys. Rev.* E **61** 493
[34] Rapini A 1975 *Can. J. Phys.* **53** 968